International Communications in Heat and Mass Transfer 158 (2024) 107889

Contents lists available at ScienceDirect

International Communications in Heat and Mass Transfer

journal homepage: www.elsevier.com/locate/ichmt

An inverse algorithm for contact heat conduction problems with an interfacial heat source based on a first-order thermocouple model

Oleksii Nosko

Gdansk University of Technology, Faculty of Mechanical Engineering and Ship Technology, ul. G. Narutowicza 11/12, Gdansk 80-233, Poland

ARTICLE INFO

Keywords:
Inverse heat conduction
Contact heat conduction
Interfacial heat source
First-order model
Noise robustness

ABSTRACT

Inverse problems of contact heat conduction with an interfacial heat source are common in various fields of science, engineering and technology. In this study, an algorithm for their solution is developed based on an inverse parametric optimisation method with an impulse response function describing the heat partition and contact heat transfer. A first-order thermocouple model with a time constant parameter is embedded in the impulse response function. The specific power of the heat source is sought in the form of a polynomial from the condition of least-squares deviation of the simulated temperature from the temperature samples obtained by a thermocouple. Compared to the classical methods of simple inverse convolution and sequential function specification, the algorithm proves to be accurate in a substantially larger region of variation of the heating duration and time constant, covering slow-response thermocouple measurements. Additionally, the algorithm is significantly more robust against noise with a sufficient number of temperature samples. The applicability of the algorithm is demonstrated by solving inverse problems of contact heat conduction typical for sliding friction, laser and electric resistance welding at different thermal contact conditions and ratios of the time constant to the heating duration.

Notation

h	measuring junction location, m
i	imaginary unit, $i = \sqrt{-1}$
k	thermal diffusivity, m^2/s
n	specific power function degree plus one
p	number of temperature samples
q	heat source specific power, W/m^2
q_{max}	maximum specific power, W/m^2
s	Laplace transform parameter
t	time variable, s
t_s	heating duration, s
x	spatial coordinate, m
B	dimensionless contact heat transfer coefficient, $B = \gamma h/K_1$
K	thermal conductivity, W/(m °C)
Q	dimensionless specific power, $Q = q/q_{max}$
T	temperature, °C
T_i	initial temperature, °C
T_m	measured temperature, °C
α	heat generation coefficient
γ	contact heat transfer coefficient, $W/(m^2\,°C)$
η	dimensionless time variable, $\eta = k_1 t/h^2$
η_r	dimensionless discrete time
η_s	dimensionless heating duration, $\eta_s = k_1 t_s/h^2$
ϑ	dimensionless temperature, $\vartheta = K_1(T - T_{i1})/(hq_{max})$
ϑ_m	dimensionless measured temperature, $\vartheta_m = K_1(T_m - T_{i1})/(hq_{max})$
ϑ_0	dimensionless initial temperature of body 2, $\vartheta_0 = K_1(T_{i2} - T_{i1})/(hq_{max})$
ξ	dimensionless spatial coordinate, $\xi = x/h$
τ	thermocouple time constant, s
χ	thermal diffusivity ratio, $\chi = k_2/k_1$
Δ	dimensionless time step
Θ	dimensionless time constant, $\Theta = k_1\tau/h^2$
Λ	thermal conductivity ratio, $\Lambda = K_2/K_1$
Ψ	dimensionless impulse response function
$\mathscr{L}[\bullet]$	Laplace transform operator
$\widetilde{\blacksquare}$	Laplace transform image
$\blacksquare_1$	related to body 1
$\blacksquare_2$	related to body 2
$\blacksquare_{1,2}$	related to bodies 1 and 2
$\blacksquare^*$	optimal/rational value

E-mail address: oleksii.nosko@pg.edu.pl.

https://doi.org/10.1016/j.icheatmasstransfer.2024.107889

Available online 8 August 2024

erfc(•)	complementary error function
exp(•)	exponential function
IPOM	inverse parametric optimisation method
SFSM	sequential function specification method
SICM	simple inverse convolution method

1. Introduction

Whenever two bodies are in mechanical contact, heat is transferred between them by various mechanisms, with an inevitable contribution of the heat conduction. This leads to temperature changes in the bodies affecting almost all processes, including mechanical, thermal, electromagnetic, chemical and biological processes. The problem of contact heat conduction, involving the determination of contact temperatures and heat fluxes, is therefore essential from both a theoretical and practical point of view.

In many technical applications and technological processes, such as sliding friction, machining and welding, the interfacial region between the contacting bodies is subjected to intensive heating accompanied by the action of aggressive factors, e.g. mechanical deformations, material removal, phase transitions or electromagnetic pulses. This means that the sensing element of a temperature sensor must not be located directly at the interface, as otherwise its function would be impaired. On the other hand, the use of non-contact measurement methods such as infrared thermography is limited by the fact that the interface is hidden between the bodies which are generally not transparent. For example, the friction pad of a disc brake may be several millimetres worn, implying that the temperature sensor cannot be installed at a smaller initial distance from the friction surface. Another example is welding, where metallic pieces heated in their interfacial region can melt at a temperature exceeding the upper measurement limit of the temperature sensor. This is where inverse heat transfer methods come into play which aim to reconstruct the contact temperatures and heat fluxes from the readings of a temperature sensor whose sensing element is located at a safe distance from the interface.

Hundreds of publications deal with inverse heat conduction problems in various fields of science, engineering and technology, as reported by Beck et al. [1], Woodbury et al. [2] and Zálešák et al. [3]. However, very few of them are devoted to the heat conduction study in the coupled formulation, i.e. the reconstruction of temperatures and heat fluxes in both bodies caused by a heat source acting at their interface. Chen et al. [4] reconstructed the friction heat generation between two sliding cylindrical bars using the conjugate gradient method and discrepancy principle. A similar approach was used by Wang et al. [5] for a semispace sliding against a plane-parallel layer and by Chen and Yang [6] for two semispaces one of which is covered by a plane-parallel layer. Bauzin et al. [7] carried out theoretical and experimental estimates of the heat flux generated by friction in a multi-disc aircraft brake, considering the imperfection of thermal friction contacts. Bauzin et al. [8] and Cherikh et al. [9] investigated the heat generation and imperfect thermal contact parameters in a friction pair consisting of a hollow steel cylinder and a bronze cylinder based on the experimental data and finite-difference analysis. Gostimirovic et al. [10] performed numerical simulations and experiments to improve the productivity and quality of grinding by finding the optimal heating regime for the workpiece–wheel contact.

The inverse problem of contact heat conduction becomes more difficult if the duration of the interfacial heat source is short. For example, in welding processes based on the laser, electrical resistance or electromagnetic principle, a single heat pulse may last 0.1 s or less. In this case, measurements with a temperature sensor are affected by its thermal inertia caused by transient heat transfer in the sensing element, thermal contact resistance between the sensing element and measurand, heat transfer in the wires, delays in signal processing, etc. Woodbury [11] showed a strong influence of the dynamics of the thermocouple sensor on the accuracy of reconstruction of the surface heat flux with a first-order model. Augustin et al. [12] used the first-order thermocouple model in a numerical algorithm to predict fluid temperatures in combustion engine exhaust systems. Frankel and Chen [13] developed and validated an inverse method by incorporating the first-order thermocouple model into an analytical temperature expression for a heated semispace. Nosko and Tsybrii [14] applied a similar approach to reconstruct the surface temperature of a pin sample sliding against a disc. Oliveira et al. [15] proposed a correction method for thermocouple measurements to avoid underestimation of boundary heat fluxes due to a delayed temperature response and applied it to a large-scale jet cooling of a hot plate. Gomez et al. [16] analysed the influence of different factors on the heat flux determination with particular attention to the thermal contact resistance of a thermal paste around the thermocouple measuring junction. The first-order model has been used extensively to evaluate the performance of different types of thermocouples when measuring temperatures at grinding contacts (Nee and Tay [17], Lefebvre et al. [18]), in flames (Santoni et al. [19], Huang et al. [20]), in fluids (Jaremkiewicz et al. [21], Zhang et al. [22]), in impingement heat transfer (Terzis et al. [23]), in reactor cores (Sylvia et al. [24], Sridhar et al. [25]), etc. With one parameter — the time constant, the first-order model allows the response of a temperature sensor to be described in the simplest way. As can be seen from the literature, this model has been used in inverse heat conduction methods. Note that more complex thermocouple models are also known. Tagawa and Ohta [26], for example, used a two-thermocouple probe for temperature measurements during combustion, assuming that the time constant of the thermocouple can vary depending on the flow and temperature conditions. Taler et al. [27] used a second-order differential equation to describe the dynamic response of a temperature sensor in a heavy thermowell.

The present study develops an algorithm to solve inverse problems of contact heat conduction with an interfacial heat source. Following the theoretical approach presented by Frankel and Chen [13], the algorithm uses an impulse response function in which the first-order thermocouple model is embedded. The impulse response function is derived for two bodies coupled with the imperfect thermal contact conditions taking into account the heat partition and contact heat transfer. The properties of the algorithm, including the solution stability, accuracy and noise robustness, are systematically investigated. Its applicability is demonstrated by solving practical problems.

2. Direct problem of contact heat conduction

Consider a body 1 ($x > 0$) with thermal conductivity K_1 and diffusivity k_1 and a body 2 ($x < 0$) with thermal conductivity K_2 and diffusivity k_2, as shown in Fig. 1. Temperatures $T_{1,2}(x,t)$ in the bodies change in time t according to the heat conduction equations

$$\begin{aligned} &\frac{\partial T_1}{\partial t} = k_1 \frac{\partial^2 T_1}{\partial x^2},\ x > 0,\ 0 < t \le t_s; \\ &\frac{\partial T_2}{\partial t} = k_2 \frac{\partial^2 T_2}{\partial x^2},\ x < 0,\ 0 < t \le t_s \end{aligned} \tag{1}$$

where t_s is the heating duration.

At initial time $t = 0$, the bodies have uniformly distributed but different temperatures T_{i1} and T_{i2}, i.e.

$$\begin{aligned} &T_1|_{t=0} = T_{i1}; \\ &T_2|_{t=0} = T_{i2} \end{aligned} \tag{2}$$

A heat source with specific power $q(t)$ acts at the interface $x = 0$. Assume an imperfect thermal contact defined by the conditions

$$\begin{aligned} &-K_1 \left.\frac{\partial T_1}{\partial x}\right|_{x=0} = \alpha q + \gamma (T_2 - T_1)|_{x=0}; \\ &K_2 \left.\frac{\partial T_2}{\partial x}\right|_{x=0} = (1-\alpha) q - \gamma (T_2 - T_1)|_{x=0} \end{aligned} \tag{3}$$

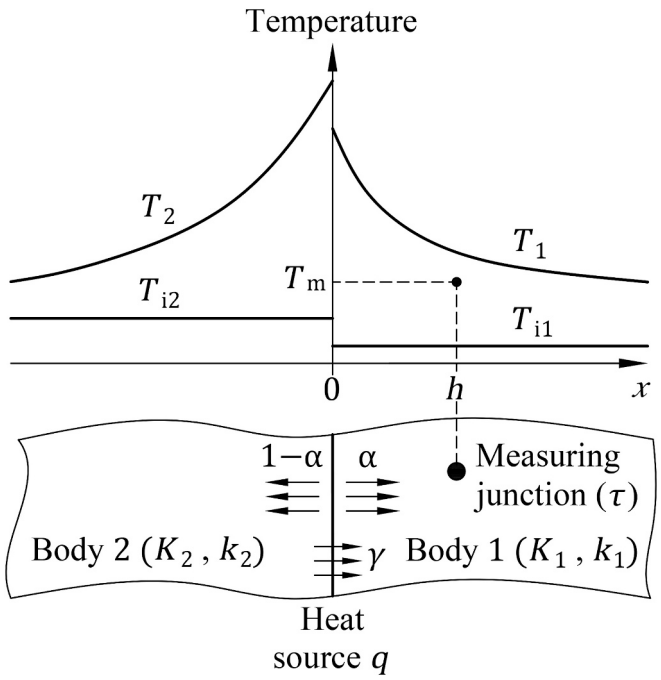

Fig. 1. Schematic of the contact heat conduction problem

where α is the heat generation coefficient; γ is the contact heat transfer coefficient. Obviously, Eq.(3) fulfils the heat balance condition. The coefficient α is responsible for the partition of the generated heat, while the coefficient γ specifies the intensity of the contact heat transfer due to the temperature jump $(T_2 - T_1)$ at the interface.

The temperatures are undisturbed at infinite distance, which is described by the conditions

$$\left.\frac{\partial T_1}{\partial x}\right|_{x\to+\infty} = \left.\frac{\partial T_2}{\partial x}\right|_{x\to-\infty} = 0 \tag{4}$$

Thereby, Eqs.(1)–(4) imply two factors affecting the temperature distributions $T_{1,2}$, namely the interfacial heat source q and initial temperature difference $(T_{i2} - T_{i1})$.

Take a polynomial specific power of the heat source in the form

$$q = q_{max}\sum_{j=1}^{n} a_j t^{j-1},\ 0 < t \le t_s \tag{5}$$

where n is the number of coefficients equal to the degree of the specific power function q plus one; a_j is the j-th coefficient; q_{max} is the maximum value of the specific power q in the considered time interval from zero to t_s.

Further, consider a thermocouple installed in the body 1 with its measuring junction at distance h from the interface (see Fig. 1). The thermocouple response is assumed to be governed by the first-order model, i.e. the measured temperature $T_m(t)$ is related to the temperature T_1 at $x = h$ according to the equation

$$\tau\frac{dT_m}{dt} + T_m = T_1|_{x=h},\ 0 < t \le t_s \tag{6}$$

where τ is the thermocouple time constant.

Naturally, the initial temperature of the measuring junction is equal to the initial temperature of the body 1, i.e.

$$T_m|_{t=0} = T_{i1} \tag{7}$$

The problem of contact heat conduction given by Eqs.(1)–(7) thus defines the relation between the heat source specific power q, initial temperature difference $(T_{i2} - T_{i1})$ and measured temperature T_m depending on many parameters: $K_{1,2}$, $k_{1,2}$, α, γ, $T_{i1,2}$, t_s, q_{max}, a_j, h and τ. It can be considerably simplified with the help of dimensionless variables

$$\xi = \frac{x}{h},\ \eta = \frac{k_1 t}{h^2},\ \vartheta_{1,2} = \frac{K_1(T_{1,2} - T_{i1})}{hq_{max}},$$
$$\vartheta_m = \frac{K_1(T_m - T_{i1})}{hq_{max}},\ Q = \frac{q}{q_{max}}$$

and parameters

$$\Lambda = \frac{K_2}{K_1},\ \chi = \frac{k_2}{k_1},\ B = \frac{\gamma h}{K_1},\ \vartheta_0 = \frac{K_1(T_{i2} - T_{i1})}{hq_{max}},\ \eta_s = \frac{k_1 t_s}{h^2},\ \Theta = \frac{k_1\tau}{h^2}$$

The dimensionless representation of Eqs.(1)–(4) reads

$$\begin{aligned}
&\frac{\partial\vartheta_1}{\partial\eta} = \frac{\partial^2\vartheta_1}{\partial\xi^2},\ \xi > 0,\ 0 < \eta \le \eta_s;\\
&\frac{\partial\vartheta_2}{\partial\eta} = \chi\frac{\partial^2\vartheta_2}{\partial\xi^2},\ \xi < 0,\ 0 < \eta \le \eta_s;\\
&\vartheta_1|_{\eta=0} = 0;\\
&\vartheta_2|_{\eta=0} = \vartheta_0;\\
&-\left.\frac{\partial\vartheta_1}{\partial\xi}\right|_{\xi=0} = \alpha Q + B(\vartheta_2 - \vartheta_1)|_{\xi=0};\\
&\Lambda\left.\frac{\partial\vartheta_2}{\partial\xi}\right|_{\xi=0} = (1-\alpha)Q - B(\vartheta_2 - \vartheta_1)|_{\xi=0};\\
&\left.\frac{\partial\vartheta_1}{\partial\xi}\right|_{\xi\to+\infty} = \left.\frac{\partial\vartheta_2}{\partial\xi}\right|_{\xi\to-\infty} = 0
\end{aligned} \tag{8}$$

while the specific power of Eq.(5) has the form

$$Q = \sum_{j=1}^{n}\mu_j\eta^{j-1} \tag{9}$$

where

$$\mu_j = a_j\left(\frac{h^2}{k_1}\right)^{j-1},\ j = 1,\ldots,n$$

The thermocouple response due to Eq.(6) and Eq.(7) transforms into

$$\begin{aligned}
&\Theta\frac{d\vartheta_m}{d\eta} + \vartheta_m = \vartheta_1|_{\xi=1},\ 0 < \eta \le \eta_s;\\
&\vartheta_m|_{\eta=0} = 0
\end{aligned} \tag{10}$$

By applying the Laplace integral transform $\mathscr{L}$ with respect to the time variable η (Doetsch [28]) as

$$\widetilde{\vartheta}_{1,2}(\xi, s) = \mathscr{L}\left[\vartheta_{1,2}(\xi,\eta)\right]$$

it is possible to represent Eq.(8) in the space of images as

$$\begin{aligned}
&\frac{\partial^2\widetilde{\vartheta}_1}{\partial\xi^2} - s\widetilde{\vartheta}_1 = 0,\ \xi > 0;\\
&\chi\frac{\partial^2\widetilde{\vartheta}_2}{\partial\xi^2} - s\widetilde{\vartheta}_2 = -\vartheta_0,\ \xi < 0;\\
&-\left.\frac{\partial\widetilde{\vartheta}_1}{\partial\xi}\right|_{\xi=0} = \alpha\widetilde{Q} + B\left(\widetilde{\vartheta}_2 - \widetilde{\vartheta}_1\right)\Big|_{\xi=0};\\
&\Lambda\left.\frac{\partial\widetilde{\vartheta}_2}{\partial\xi}\right|_{\xi=0} = (1-\alpha)\widetilde{Q} - B\left(\widetilde{\vartheta}_2 - \widetilde{\vartheta}_1\right)\Big|_{\xi=0};\\
&\left.\frac{\partial\widetilde{\vartheta}_1}{\partial\xi}\right|_{\xi\to+\infty} = \left.\frac{\partial\widetilde{\vartheta}_2}{\partial\xi}\right|_{\xi\to-\infty} = 0
\end{aligned} \tag{11}$$

while the image of the specific power of Eq.(9) is written as

$$\widetilde{Q}(s)=\mathscr{L}[Q(\eta)]=\sum_{j=1}^{n}\frac{\mu_j(j-1)!}{s^j} \tag{12}$$

where s is the parameter of the Laplace transform.

The temperature images $\widetilde{\vartheta}_{1,2}$ result from Eq.(11) and Eq.(12) in the form

$$\begin{aligned}\widetilde{\vartheta}_1&=\sum_{j=1}^{n}\frac{\mu_j(j-1)!\left(\alpha\Lambda\sqrt{s}+B\sqrt{\chi}\right)}{s^{1/2+j}\left(\Lambda\sqrt{s}+B\left(\Lambda+\sqrt{\chi}\right)\right)}exp\{-\xi\sqrt{s}\}\\&+\frac{\vartheta_0 B\Lambda}{s\left(\Lambda\sqrt{s}+B\left(\Lambda+\sqrt{\chi}\right)\right)}exp\{-\xi\sqrt{s}\};\\\widetilde{\vartheta}_2&=\sum_{j=1}^{n}\frac{\mu_j(j-1)!\left((1-\alpha)\sqrt{\chi}\sqrt{s}+B\sqrt{\chi}\right)}{s^{1/2+j}\left(\Lambda\sqrt{s}+B\left(\Lambda+\sqrt{\chi}\right)\right)}exp\left\{\frac{\xi}{\sqrt{\chi}}\sqrt{s}\right\}\\&+\vartheta_0\left(\frac{1}{s}-\frac{B\sqrt{\chi}}{s\left(\Lambda\sqrt{s}+B\left(\Lambda+\sqrt{\chi}\right)\right)}exp\left\{\frac{\xi}{\sqrt{\chi}}\sqrt{s}\right\}\right)\end{aligned} \tag{13}$$

In both expressions of Eq.(13), the first term describes the influence of the heat source, while the second term represents the contact heat transfer due to the initial temperature difference. Note that Eq.(13) can be derived as a superposition of the long-known expressions obtained by Schaaf [29] for two semispaces coupled with the imperfect thermal contact conditions equivalent to Eq.(3) and by Mersman [30] for the heat transfer between the semispaces in the presence of a thermal contact resistance.

Finally, the transform

$$\widetilde{\vartheta}_{\mathrm{m}}(s)=\mathscr{L}[\vartheta_{\mathrm{m}}(\eta)]$$

of Eq.(10) leads to the measured temperature image

$$\begin{aligned}\widetilde{\vartheta}_{\mathrm{m}}&=\frac{\alpha}{\Theta}\sum_{j=1}^{n}\frac{\mu_j(j-1)!\left(\sqrt{s}+B\sqrt{\chi}/(\alpha\Lambda)\right)exp\{-\sqrt{s}\}}{s^{1/2+j}\left(\sqrt{s}+B\left(1+\sqrt{\chi}/\Lambda\right)\right)(s+\Theta^{-1})}\\&+\frac{\vartheta_0 B exp\{-\sqrt{s}\}}{\Theta s\left(\sqrt{s}+B\left(1+\sqrt{\chi}/\Lambda\right)\right)(s+\Theta^{-1})}\end{aligned} \tag{14}$$

The known transform (Carslaw and Jaeger [31]) of

$$\begin{aligned}&\mathscr{L}^{-1}\left[\frac{exp\{-\sqrt{s}\}}{(\sqrt{s}+b)(s-c)}\right]\\&=\frac{exp\{c\eta\}}{2}\left(\frac{exp\{-\sqrt{c}\}}{b+\sqrt{c}}erfc\left\{\frac{1}{2\sqrt{\eta}}-\sqrt{c\eta}\right\}\right.\\&\left.+\frac{exp\{\sqrt{c}\}}{b-\sqrt{c}}erfc\left\{\frac{1}{2\sqrt{\eta}}+\sqrt{c\eta}\right\}\right)\\&-\frac{bexp\{b(1+b\eta)\}}{b^2-c}erfc\left\{\frac{1}{2\sqrt{\eta}}+b\sqrt{\eta}\right\}\end{aligned} \tag{15}$$

allows obtaining useful transforms

$$\begin{aligned}&\mathscr{L}^{-1}\left[\frac{exp\{-\sqrt{s}\}}{\sqrt{s}(\sqrt{s}+b)(s-c)}\right]\\&=\frac{exp\{c\eta\}}{2\sqrt{c}}\left(\frac{exp\{-\sqrt{c}\}}{b+\sqrt{c}}erfc\left\{\frac{1}{2\sqrt{\eta}}-\sqrt{c\eta}\right\}\right.\\&\left.-\frac{exp\{\sqrt{c}\}}{b-\sqrt{c}}erfc\left\{\frac{1}{2\sqrt{\eta}}+\sqrt{c\eta}\right\}\right)\\&+\frac{exp\{b(1+b\eta)\}}{b^2-c}erfc\left\{\frac{1}{2\sqrt{\eta}}+b\sqrt{\eta}\right\}\end{aligned} \tag{16}$$

and

$$\begin{aligned}&\mathscr{L}^{-1}\left[\frac{exp\{-\sqrt{s}\}}{s(\sqrt{s}+b)(s-c)}\right]\\&=\frac{exp\{c\eta\}}{2c}\left(\frac{exp\{-\sqrt{c}\}}{b+\sqrt{c}}erfc\left\{\frac{1}{2\sqrt{\eta}}-\sqrt{c\eta}\right\}\right.\\&\left.+\frac{exp\{\sqrt{c}\}}{b-\sqrt{c}}erfc\left\{\frac{1}{2\sqrt{\eta}}+\sqrt{c\eta}\right\}\right)\\&-\frac{exp\{b(1+b\eta)\}}{b(b^2-c)}erfc\left\{\frac{1}{2\sqrt{\eta}}+b\sqrt{\eta}\right\}-\frac{1}{bc}erfc\left\{\frac{1}{2\sqrt{\eta}}\right\}\end{aligned} \tag{17}$$

where $erfc(\bullet)$ is the complementary error function; b and c are real.

The transforms of Eqs.(15)–(17) at $b=B\left(1+\sqrt{\chi}/\Lambda\right)$ and $c=-\Theta^{-1}$ enable finding the original of Eq.(14) in the form

$$\vartheta_{\mathrm{m}}=\sum_{j=1}^{n}\mu_j\Psi_j+\Phi \tag{18}$$

where the impulse response function $\Psi(\eta)$ and the function $\Phi(\eta)$ representing the initial temperature difference are expressed as

$$\begin{aligned}\Psi&=\frac{\alpha\Lambda i+B\sqrt{\chi\Theta}}{2\left(B\Theta\left(\Lambda+\sqrt{\chi}\right)i-\Lambda\sqrt{\Theta}\right)}exp\left\{-\frac{\eta}{\Theta}-\frac{i}{\sqrt{\Theta}}\right\}\\&\times erfc\left\{\frac{1}{2\sqrt{\eta}}-\frac{i\sqrt{\eta}}{\sqrt{\Theta}}\right\}+\frac{\alpha\Lambda i-B\sqrt{\chi\Theta}}{2\left(B\Theta\left(\Lambda+\sqrt{\chi}\right)i+\Lambda\sqrt{\Theta}\right)}\\&\times exp\left\{-\frac{\eta}{\Theta}+\frac{i}{\sqrt{\Theta}}\right\}erfc\left\{\frac{1}{2\sqrt{\eta}}+\frac{i\sqrt{\eta}}{\sqrt{\Theta}}\right\}\\&+\frac{B\Lambda\left(\sqrt{\chi}-\alpha\left(\Lambda+\sqrt{\chi}\right)\right)}{\Lambda^2+\Theta B^2\left(\Lambda+\sqrt{\chi}\right)^2}exp\left\{\frac{B\left(\Lambda+\sqrt{\chi}\right)}{\Lambda^2}\left(\Lambda+B\left(\Lambda+\sqrt{\chi}\right)\eta\right)\right\}\\&\times erfc\left\{\frac{1}{2\sqrt{\eta}}+\frac{B\left(\Lambda+\sqrt{\chi}\right)}{\Lambda}\sqrt{\eta}\right\};\\\Phi&=\frac{\vartheta_0\Lambda}{\Lambda+\sqrt{\chi}}erfc\left\{\frac{1}{2\sqrt{\eta}}\right\}\\&-\frac{\vartheta_0 B\Lambda\sqrt{\Theta}}{2\left(B\left(\Lambda+\sqrt{\chi}\right)\sqrt{\Theta}+\Lambda i\right)}exp\left\{-\frac{\eta}{\Theta}-\frac{i}{\sqrt{\Theta}}\right\}erfc\left\{\frac{1}{2\sqrt{\eta}}-\frac{i\sqrt{\eta}}{\sqrt{\Theta}}\right\}\\&-\frac{\vartheta_0 B\Lambda\sqrt{\Theta}}{2\left(B\left(\Lambda+\sqrt{\chi}\right)\sqrt{\Theta}-\Lambda i\right)}exp\left\{-\frac{\eta}{\Theta}+\frac{i}{\sqrt{\Theta}}\right\}erfc\left\{\frac{1}{2\sqrt{\eta}}+\frac{i\sqrt{\eta}}{\sqrt{\Theta}}\right\}\\&-\frac{\vartheta_0\Lambda^3}{\left(\Lambda+\sqrt{\chi}\right)\left(\Lambda^2+\Theta B^2\left(\Lambda+\sqrt{\chi}\right)^2\right)}\\&\times exp\left\{\frac{B\left(\Lambda+\sqrt{\chi}\right)}{\Lambda^2}\left(\Lambda+B\left(\Lambda+\sqrt{\chi}\right)\eta\right)\right\}\\&\times erfc\left\{\frac{1}{2\sqrt{\eta}}+\frac{B\left(\Lambda+\sqrt{\chi}\right)}{\Lambda}\sqrt{\eta}\right\}\end{aligned} \tag{19}$$

while the subscript of Ψ in Eq.(18) indicates repeated integration by the rule

$$\Psi_j(\eta)=(j-1)!\underbrace{\int_0^{\eta}\dots\int_0^{\eta}}_{j}\Psi(\varsigma)\underbrace{d\varsigma\dots d\varsigma}_{j} \tag{20}$$

The functions Ψ and Φ given by Eq.(19) take real values, although they contain the imaginary unit $i=\sqrt{-1}$. Appendix **A** provides the analytical expressions Ψ_j due to Eq.(20) which allow the specific power Q to be defined as a polynomial of degree up to and including 9.

The analytical solution for the direct problem of contact heat con-

duction is thus given by Eq.(18). Although this solution is based on the classical mathematical methods, it is additionally validated by comparisons with the numerical solutions obtained by the Crank–Nicolson implicit method in order to avoid accidental errors. Fig. 2 shows such comparisons for constant, linear and quadratic specific power Q at $\Lambda = 2$, $\chi = 3$, $\alpha = 1/4$, $B = 5$, $\vartheta_0 = 1$, $\Theta = 6$ and $\eta_s = 10$.

3. Particular cases of the contact heat conduction problem

The important particular cases differing in the thermal contact conditions are considered. The asymptotic analysis of Eq.(18) is cumbersome due to the complex-structured functions Ψ and Φ. A more efficient approach is to find the limit expression of the image given by Eq.(14) and then perform its inverse transform.

The imperfect thermal contact conditions of Eq.(3) generalise several well-known types of thermal contact, as reviewed by Yevtushenko and Kuciej [32] and Nosko [33]. As $B\to 0$, there is no contact heat transfer between the bodies, and Eq.(14) simplifies to the expression

$$\widetilde{\vartheta}_{\mathrm{m}} = \frac{\alpha}{\Theta}\sum_{j=1}^{n}\frac{\mu_j (j-1)!exp\{-\sqrt{s}\}}{s^{1/2+j}(s+\Theta^{-1})}$$

which, according to Eq.(15), corresponds to the functions

$$\begin{aligned}\Psi &= \frac{\alpha i}{2\sqrt{\Theta}}\left(exp\left\{-\frac{\eta}{\Theta}+\frac{i}{\sqrt{\Theta}}\right\}erfc\left\{\frac{1}{2\sqrt{\eta}}+\frac{i\sqrt{\eta}}{\sqrt{\Theta}}\right\}\right.\\ &\left.-exp\left\{-\frac{\eta}{\Theta}-\frac{i}{\sqrt{\Theta}}\right\}erfc\left\{\frac{1}{2\sqrt{\eta}}-\frac{i\sqrt{\eta}}{\sqrt{\Theta}}\right\}\right);\\ \Phi &= 0\end{aligned} \tag{21}$$

Note that the expressions equivalent to Ψ in Eq.(21) were previously derived by Frankel and Chen [13] and Nosko and Tsybrii [14].

On the other hand, when $B\to\infty$, Eq.(3) degrades to the perfect thermal contact conditions, implying temperature continuity at the interface, while Eq.(14) transforms into

$$\widetilde{\vartheta}_{\mathrm{m}} = \frac{\sqrt{\chi}}{\Theta(\Lambda+\sqrt{\chi})}\sum_{j=1}^{n}\frac{\mu_j (j-1)!exp\{-\sqrt{s}\}}{s^{1/2+j}(s+\Theta^{-1})}+\frac{\vartheta_0\Lambda exp\{-\sqrt{s}\}}{\Theta(\Lambda+\sqrt{\chi})s(s+\Theta^{-1})}$$

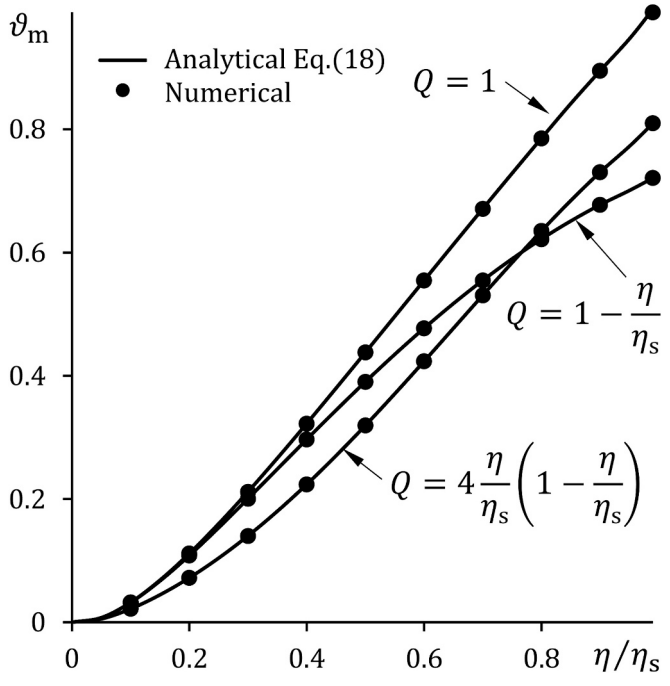

Fig. 2. Validation of the contact heat conduction problem solution

or, in the space of originals,

$$\begin{aligned}\Psi &= \frac{i\sqrt{\chi}}{2\sqrt{\Theta}(\Lambda+\sqrt{\chi})}\left(exp\left\{-\frac{\eta}{\Theta}+\frac{i}{\sqrt{\Theta}}\right\}erfc\left\{\frac{1}{2\sqrt{\eta}}+\frac{i\sqrt{\eta}}{\sqrt{\Theta}}\right\}\right.\\ &\left.-exp\left\{-\frac{\eta}{\Theta}-\frac{i}{\sqrt{\Theta}}\right\}erfc\left\{\frac{1}{2\sqrt{\eta}}-\frac{i\sqrt{\eta}}{\sqrt{\Theta}}\right\}\right);\\ \Phi &= \frac{\vartheta_0\Lambda}{2(\Lambda+\sqrt{\chi})}\left(2\,erfc\left\{\frac{1}{2\sqrt{\eta}}\right\}\right.\\ &-exp\left\{-\frac{\eta}{\Theta}+\frac{i}{\sqrt{\Theta}}\right\}erfc\left\{\frac{1}{2\sqrt{\eta}}+\frac{i\sqrt{\eta}}{\sqrt{\Theta}}\right\}\\ &\left.-exp\left\{-\frac{\eta}{\Theta}-\frac{i}{\sqrt{\Theta}}\right\}erfc\left\{\frac{1}{2\sqrt{\eta}}-\frac{i\sqrt{\eta}}{\sqrt{\Theta}}\right\}\right)\end{aligned} \tag{22}$$

In some practical situations, the temperature variation in the counter-body (body 2) can be neglected. If $\Lambda\to\infty$ is assumed, Eq.(14) simplifies to

$$\widetilde{\vartheta}_{\mathrm{m}} = \frac{\alpha}{\Theta}\sum_{j=1}^{n}\frac{\mu_j (j-1)!exp\{-\sqrt{s}\}}{s^{j}(\sqrt{s}+B)(s+\Theta^{-1})}+\frac{\vartheta_0 B exp\{-\sqrt{s}\}}{\Theta s(\sqrt{s}+B)(s+\Theta^{-1})}$$

implying

$$\begin{aligned}\Psi &= \frac{\alpha}{2\sqrt{\Theta}\left(B\sqrt{\Theta}+i\right)}exp\left\{-\frac{\eta}{\Theta}-\frac{i}{\sqrt{\Theta}}\right\}erfc\left\{\frac{1}{2\sqrt{\eta}}-\frac{i\sqrt{\eta}}{\sqrt{\Theta}}\right\}\\ &+\frac{\alpha}{2\sqrt{\Theta}\left(B\sqrt{\Theta}-i\right)}exp\left\{-\frac{\eta}{\Theta}+\frac{i}{\sqrt{\Theta}}\right\}erfc\left\{\frac{1}{2\sqrt{\eta}}+\frac{i\sqrt{\eta}}{\sqrt{\Theta}}\right\}\\ &-\frac{\alpha B}{1+\Theta B^2}exp\{B(1+B\eta)\}erfc\left\{\frac{1}{2\sqrt{\eta}}+B\sqrt{\eta}\right\};\\ \Phi &= \vartheta_0\,erfc\left\{\frac{1}{2\sqrt{\eta}}\right\}\\ &-\frac{\vartheta_0 B\sqrt{\Theta}}{2\left(B\sqrt{\Theta}+i\right)}exp\left\{-\frac{\eta}{\Theta}-\frac{i}{\sqrt{\Theta}}\right\}erfc\left\{\frac{1}{2\sqrt{\eta}}-\frac{i\sqrt{\eta}}{\sqrt{\Theta}}\right\}\\ &-\frac{\vartheta_0 B\sqrt{\Theta}}{2\left(B\sqrt{\Theta}-i\right)}exp\left\{-\frac{\eta}{\Theta}+\frac{i}{\sqrt{\Theta}}\right\}erfc\left\{\frac{1}{2\sqrt{\eta}}+\frac{i\sqrt{\eta}}{\sqrt{\Theta}}\right\}\\ &-\frac{\vartheta_0}{1+\Theta B^2}exp\{B(1+B\eta)\}erfc\left\{\frac{1}{2\sqrt{\eta}}+B\sqrt{\eta}\right\}\end{aligned} \tag{23}$$

The practical significance of Eqs.(21)–(23) is shown in the next sections.

4. Algorithm based on the inverse parametric optimisation method

The measurement data from a thermocouple represents a series of temperature samples $\vartheta_{\mathrm{m}}^{(r)}$ obtained at discrete times η_r. The sampling frequency is normally constant, implying that η_r can be defined as

$$\eta_r = \frac{\eta_s}{p}r,\ r = 1,\ldots,p$$

where p is the number of temperature samples $\vartheta_{\mathrm{m}}^{(r)}$, which by default is set equal to 100.

According to Eq.(9), the sought specific power Q is approximated by a polynomial with n unknown coefficients μ_j. Note that the number n is also unknown a priori. Thus, the inverse problem of contact heat conduction consists in finding n and μ_j from the temperature samples $\vartheta_{\mathrm{m}}^{(r)}$ and the parameters contained in the functions Ψ and Φ. It can be solved

by the inverse parametric optimisation method (IPOM), originating from early studies by Beck [34], Frank [35] and Burggraf [36]. The root-mean-square deviation σ of the temperature ϑ_m determined by Eq.(18) at times η_r from the temperature samples $\vartheta_m^{(r)}$ tends to the minimum, i.e.

$$\sigma^2 = \frac{1}{p}\sum_{r=1}^{p}\left(\sum_{j=1}^{n}\mu_j\Psi_j(\eta_r) + \Phi(\eta_r) - \vartheta_m^{(r)}\right)^2 \rightarrow min \tag{24}$$

For a fixed value of n, taking derivative of the deviation σ with respect to each μ_j and equalising it to zero lead to the system of linear algebraic equations

$$\sum_{l=1}^{n}\sum_{r=1}^{p}\Psi_j(\eta_r)\Psi_l(\eta_r)\mu_l = \sum_{r=1}^{p}\left(\vartheta_m^{(r)} - \Phi(\eta_r)\right)\Psi_j(\eta_r),\ j = 1,\ldots,n \tag{25}$$

Solving Eq.(25) for the cyclically incremented number n makes it possible to find the parameters $n = n^*$ and μ_j providing the minimum deviation $\sigma = \sigma^*$ and reconstruct the specific power Q by Eq.(9).

Fig. 3 illustrates the application of IPOM according to Eqs.(24),(25) for a cubic specific power specified as $Q = 1 - 4(\eta/\eta_s) + 9(\eta/\eta_s)^2 - 6(\eta/\eta_s)^3$ at $\Lambda = 2, \chi = 3, \alpha = 1/4, B = 5, \vartheta_0 = 1, \Theta = 6$ and $\eta_s = 10$. It can be seen that with n from 1 to 3, the deviation σ decreases although taking a relatively large value of order 10^{-2} as the IPOM solution remains inadequate. For $n = n^* = 4$, Q is perfectly described by Eq.(9) with σ^* of order 10^{-12}. The subsequent increase in n leads to an accumulation of calculation errors and an associated increase in σ. The calculation errors originate from ill-conditioned Eq.(25), integration due to Eq.(20), rounding-off, etc.

Fig. 4 considers the general case where the specific power Q is not polynomial. It is accepted that $Q = 16/3^{3/2}(\eta/\eta_s)^{3/2}(1 - \eta/\eta_s)^{1/2}$ under the same parameters as in the previous case. As n changes from 1 to 8, the IPOM solution becomes more adequate, which is accompanied by decreasing σ. The minimum deviation σ^* of order 10^{-5} is reached at $n = n^* = 8$, providing an accurate approximation of Q by a polynomial of degree 7.

The above analysis reveals two general trends in the behaviour of the deviation σ depending on the number n. On the one hand, as n increases, the IPOM solution is able to approximate Q more accurately, implying a smaller value of σ. On the other hand, an increase in n leads to larger calculation errors and an increase in σ. The intersection of the trends corresponds to the minimum deviation σ^* at $n = n^*$. The number n thus plays the role of a regularisation parameter, similar to the Tikhonov regularisation parameter which establishes a balance between the competing effects of the bias and random errors (Woodbury and Beck [37]).

For certain parameter combinations, however, the calculation errors reach a critical level when the minimum deviation σ^* is unacceptably large and the IPOM solution is correspondingly inaccurate. Fig. 5 shows the influence of the calculation errors on the reconstruction of the sinusoidal heat pulse specified as

$$Q = sin\left(\frac{\pi\eta}{\eta_s}\right) \tag{26}$$

The IPOM solution is obtained using the function Ψ from Eq.(21) corresponding to the forced heat partition conditions at $\alpha = 1$ and $\Theta = 1$. It is shown that for $\eta_s = 100$, σ^* is of order 10^{-6}, while the IPOM solution coincides with the exact solution. In contrast, a noticeable error occurs in the IPOM solution at $\eta_s = 1000$ with σ^* of order 10^{-2}, which is due to ill-conditioned Eq.(25).

The analysis shows that if IPOM provides an accurate solution, the number n is not greater than 9. This limits the application range of IPOM to the set of specific power functions which can be approximated by a polynomial of degree up to about 8.

5. Reference inverse methods

For any specific power function Q, the contact heat conduction problem of Eq.(8) can be expressed in the form of convolution equation

$$\vartheta_m(\eta) = \int_0^{\eta} Q(\eta - \epsilon)\Psi(\epsilon)d\epsilon + \Phi(\eta) \tag{27}$$

which belongs to the family of Volterra integral equations of the first kind with difference kernel.

The introduction of time step Δ defines the discrete times $\eta_r = r\Delta$ and mid-times $\eta_{r\pm1/2} = (r \pm 1/2)\Delta$. The quadrature formula based on the trapezoidal rule transforms Eq.(27) into the equation relating the specific power $Q^{(r-1/2)}$ at the mid-times $\eta_{r-1/2}$ and the temperature samples $\vartheta_m^{(r)}$ at the times η_r as follows:

$$\vartheta_m^{(r)} = \sum_{m=1}^{r} Q^{(m-1/2)}\Delta\Psi_{r-m} + \Phi(\eta_r) \tag{28}$$

where $\Delta\Psi_{r-m}$ is obtained by integration

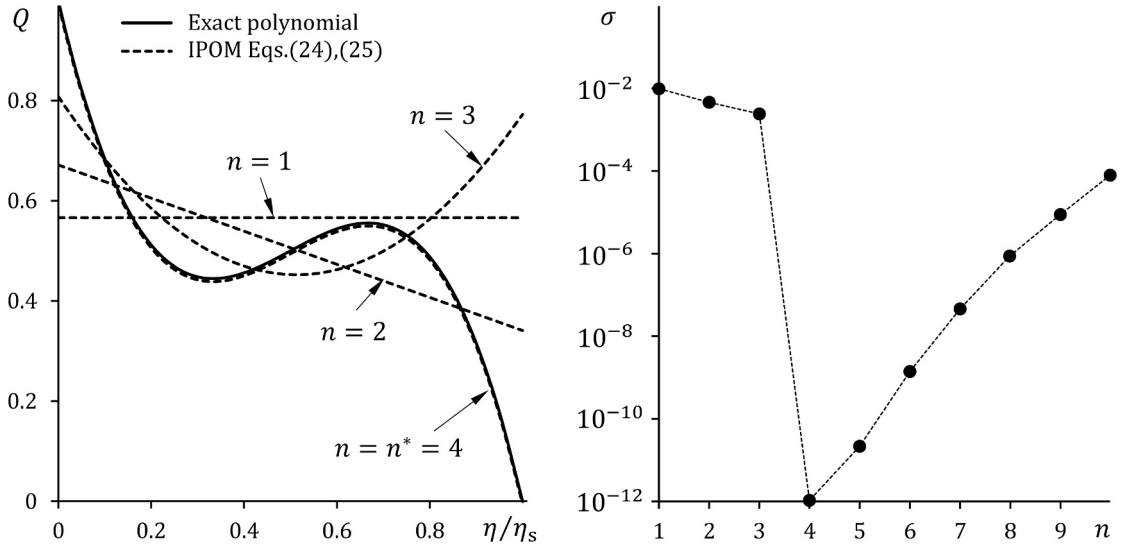

Fig. 3. Application of IPOM to reconstruct the polynomial specific power Q

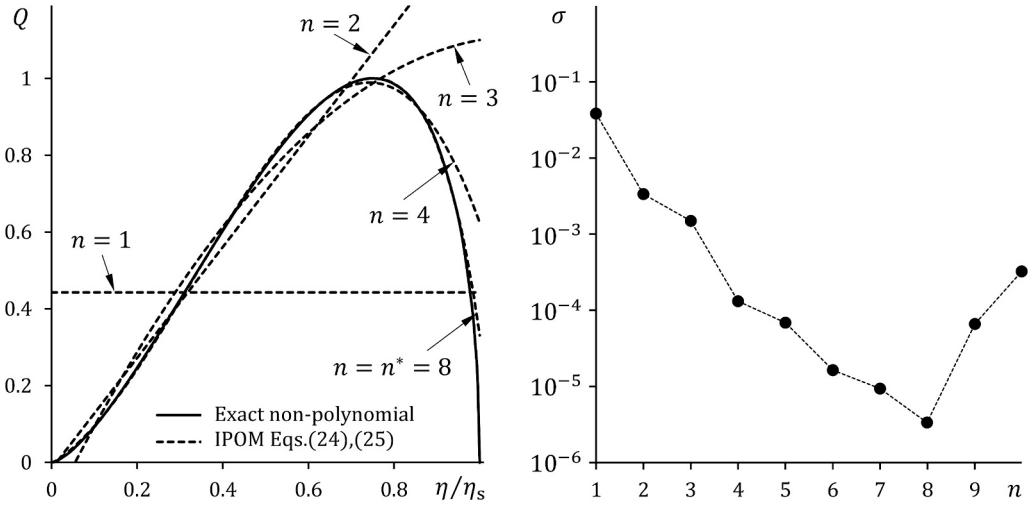

Fig. 4. Application of IPOM to reconstruct the non-polynomial specific power Q

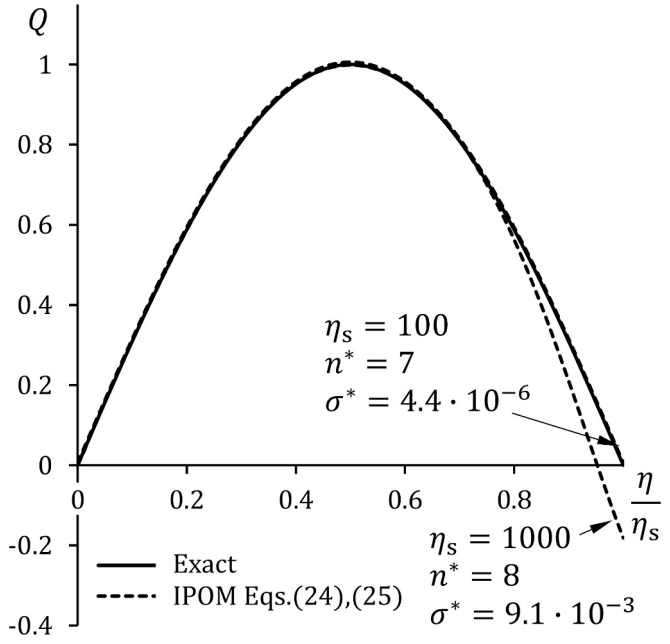

Fig. 5. Influence of the calculation errors on the IPOM solution

$$\Delta\Psi_{r-m} = \int_{\eta_{r-m}}^{\eta_{r-m+1}} \Psi(\varsigma)d\varsigma = \Psi_1(\eta_{r-m+1}) - \Psi_1(\eta_{r-m})$$

The solution of Eq.(28) is found using the recurrent formula (Stolz [38], Beck [39])

$$Q^{(r-1/2)} = \frac{1}{\Delta\Psi_0}\left(\vartheta_m^{(r)} - \Phi(\eta_r) - \sum_{m=1}^{r-1} Q^{(m-1/2)}\Delta\Psi_{r-m}\right) \quad (29)$$

After calculations with Eq.(29), the specific power $Q^{(r)}$ at the time η_r is finally determined as the average between $Q^{(r-1/2)}$ and $Q^{(r+1/2)}$. The inverse heat conduction method given by Eq.(29) is referred to as the simple inverse convolution method (SICM).

The stability and accuracy of SICM are intimately related to the specification of the time step Δ. On the one hand, the SICM solution becomes less stable with a decrease in Δ, implying the occurrence of unphysical oscillations. On the other hand, an increase in Δ leads to an oversmoothed SICM solution with a loss of physically explainable frequencies. Therefore, a rational time step Δ^* should be chosen to avoid the instability and achieve a reasonable smoothness of the SICM solution. The principle of natural step regularisation suggests that Δ^* is equal to the point of maximum of the kernel function (Alifanov [40]), i.e.

$$\Psi(\Delta^*) \rightarrow max \quad (30)$$

The instability and oversmoothing effects are illustrated for the sinusoidal heat pulse of Eq.(26). Fig. 6 shows the specific power reconstructed by Eq.(29) with Ψ given by Eq.(21) at $\alpha = 1$, $\Theta = 1$ and $\eta_s = 50$. It can be seen that the SICM solution is unstable at $\Delta = \Delta^*/2$. Further, SICM provides a sufficiently accurate solution at $\Delta = \Delta^*$. Furthermore, the SICM solution is oversmoothed at larger $\Delta = 4\Delta^*$. The following SICM simulations obey the principle of natural step regularisation due to Eq.(30).

The limitation from below on the time step Δ inherent in SICM is very impractical. Beck [41,42] proposed a generalisation of SICM that uses information about the future temperature and allows a significant reduction of the time step, the so-called sequential function specification method (SFSM). The simplest formulation of SFSM, in which only one

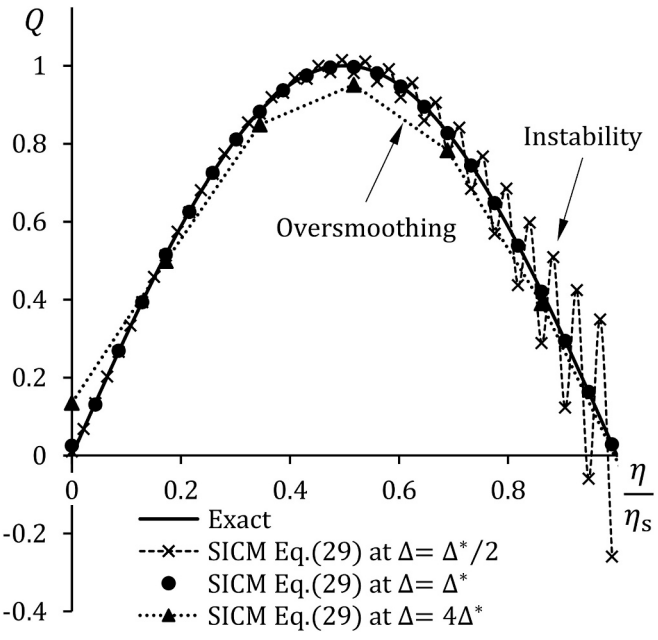

Fig. 6. Influence of the time step Δ on the SICM solution

future temperature is considered, discretises Eq.(27) for the future time $\eta_{r+1} = (r+1)\Delta$ as

$$\vartheta_{\mathrm{m}}^{(r+1)} = \sum_{m=1}^{r} Q^{(\mathrm{m}-1/2)} \Delta\Psi_{r-m+1} + Q^{(r-1/2+1)} \Delta\Psi_0 + \Phi(\eta_{r+1}) \tag{31}$$

It is also assumed that the future specific power is equal to the current specific power, i.e.

$$Q^{(r-1/2+1)} = Q^{(r-1/2)} \tag{32}$$

The condition of least-squares deviation of the temperatures given by Eq.(28) and Eq.(31) in the form

$$\sum_{l=0}^{1} \left(\sum_{m=1}^{r+l} Q^{(m-1/2)} \Delta\Psi_{r-m+l} + \Phi(\eta_{r+l}) - \vartheta_{\mathrm{m}}^{(r+l)} \right)^2 \rightarrow min$$

combined with Eq.(32) leads to the following equation:

$$\begin{aligned} Q^{(r-1/2)} = {} & \frac{\Delta\Psi_0 \vartheta_{\mathrm{m}}^{(r)} + (\Delta\Psi_0 + \Delta\Psi_1)\vartheta_{\mathrm{m}}^{(r+1)}}{(\Delta\Psi_0)^2 + (\Delta\Psi_0 + \Delta\Psi_1)^2} \\ & - \frac{\Delta\Psi_0 \Phi(\eta_r) + (\Delta\Psi_0 + \Delta\Psi_1)\Phi(\eta_{r+1})}{(\Delta\Psi_0)^2 + (\Delta\Psi_0 + \Delta\Psi_1)^2} \\ & - \sum_{m=1}^{r-1} Q^{(m-1/2)} \frac{\Delta\Psi_0 \Delta\Psi_{r-m} + (\Delta\Psi_0 + \Delta\Psi_1)\Delta\Psi_{r-m+1}}{(\Delta\Psi_0)^2 + (\Delta\Psi_0 + \Delta\Psi_1)^2} \end{aligned} \tag{33}$$

The analysis shows that SFSM given by Eq.(33) yields a stable solution at smaller time step $\Delta = \Delta^*/4$, which is used in the following simulations. The further two-fold decrease in Δ may already be accompanied by the instability effects. This agrees well with the conclusion by Beck [41] that 'the new method is stable with time steps as small as one sixth of the minimum allowable time step in the Stolz method'.

6. Accuracy and noise robustness of the algorithm

The accuracy and noise robustness of IPOM is analysed for the sinusoidal heat pulse of Eq.(26) and compared to those of SICM and SFSM. The considered problem involves two dimensionless parameters, namely the heating duration η_s and time constant Θ. IPOM uses Ψ given by Eq. (21) with $\alpha = 1$.

The accuracy of the inverse method is characterised by the root-mean-square deviation σ_Q of the reconstructed specific power Q from exact Eq.(26). Fig. 7 shows the region of accurate simulations in the plane (η_s, Θ) with $\sigma_Q < 1\%$. The solid, dashed and dotted lines correspond to IPOM, SFSM and SICM, respectively. The highlighted practical region is bounded by the line $\Theta = 100\eta_s$ (slow-response thermocouple) and $\Theta = 0.01\eta_s$ (fast-response thermocouple). For a more meaningful representation, a logarithmic scale with a base of 10 is used.

SICM is accurate within a small fraction of the practical region corresponding to fast-response thermocouple measurements. SFSM allows accurate simulations for a larger region, but still does not cover slow-response thermocouple measurements due to the oversmoothing effect. As discussed above, the oversmoothing cannot be overcome by decreasing the time step Δ as the inverse solution becomes unstable. In contrast, IPOM is accurate over a substantially larger fraction of the practical region and covers both fast- and slow-response thermocouple measurements.

The noise robustness of the inverse method is investigated by disturbing the temperature samples $\vartheta_{\mathrm{m}}^{(r)}$ with random noise with zero mean and a small standard deviation σ_ϑ and by analysing the influence on the specific power deviation σ_Q. In the analysis, the heating duration $\eta_s = 50$ and time constant $\Theta = 1$ are accepted, which, according to Fig. 7, correspond to the stable and accurate solutions by the three inverse methods for the undisturbed measured temperature. Table 1 shows the obtained statistical data, where the deviation σ_Q is the mean value for a cycle of 1000 simulations, while the ratio $\sigma_Q/\sigma_\vartheta$ is used to characterise the noise sensitivity of the inverse methods. The presented values of σ_Q are repeatable from cycle to cycle of the simulations.

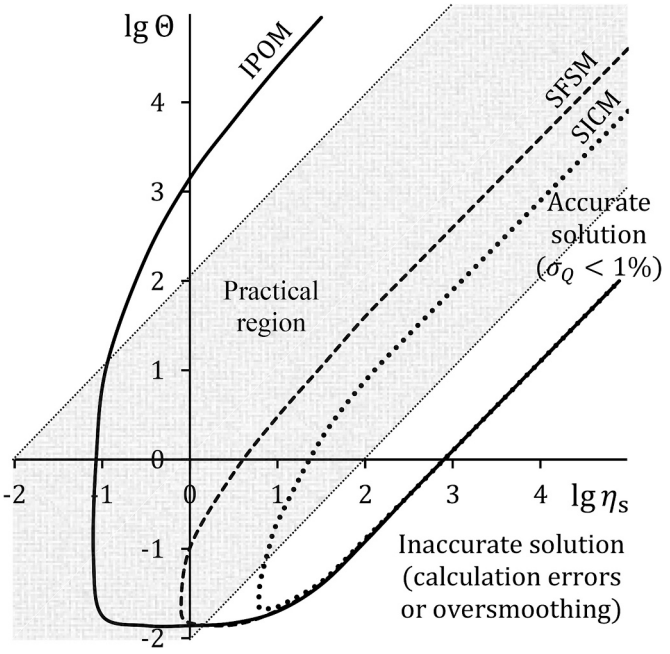

Fig. 7. Accuracy of the inverse methods for the sinusoidal heat pulse

Table 1
Noise sensitivity of the inverse methods for the sinusoidal heat pulse

σ_ϑ	Inverse method	σ_Q	$\sigma_Q/\sigma_\vartheta$
	SICM	0.0028	2.8
	SFSM	0.0041	4.1
$10^{-3} \pm 10^{-5}$	IPOM at $p = 10$ ($n^* = 5$)	0.00094	0.94
	IPOM at $p = 10^2$ ($n^* = 7$)	0.00031	0.31
	IPOM at $p = 10^3$ ($n^* = 7$)	0.00011	0.11
	SICM	0.0099	0.99
	SFSM	0.040	4.0
$10^{-2} \pm 10^{-4}$	IPOM at $p = 10$ ($n^* = 5$)	0.0054	0.54
	IPOM at $p = 10^2$ ($n^* = 5$)	0.0017	0.17
	IPOM at $p = 10^3$ ($n^* = 5$)	0.00069	0.069
	SICM	0.097	0.97
	SFSM	0.40	4.0
$10^{-1} \pm 10^{-3}$	IPOM at $p = 10$ ($n^* = 3$)	0.034	0.34
	IPOM at $p = 10^2$ ($n^* = 5$)	0.016	0.16
	IPOM at $p = 10^3$ ($n^* = 5$)	0.0054	0.054

According to Table 1, SICM is sensitive to noise with $\sigma_Q/\sigma_\vartheta$ of about 1–3. SFSM is more noise sensitive with $\sigma_Q/\sigma_\vartheta \approx 4$ (at $\Delta = \Delta^*/4$). The noise sensitivity of IPOM decreases with an increase in the number p of temperature samples or with an increase in the standard deviation σ_ϑ. For small $p = 10$, IPOM has the ratio $\sigma_Q/\sigma_\vartheta$ which is comparable to the ratio $\sigma_Q/\sigma_\vartheta$ for SICM. However, with an increase in p to 1000, $\sigma_Q/\sigma_\vartheta$ becomes an order of magnitude smaller. At $\sigma_\vartheta = 0.1$, for example, it is only 0.054.

Compared to SICM and SFSM, IPOM thus exhibits a significantly higher robustness against noise, especially for large p. This finding can be explained by the fact that the larger is p, the smaller is the influence of a single noise-induced deviation in the temperature samples $\vartheta_{\mathrm{m}}^{(r)}$ on the reconstruction of the specific power Q. In other words, the filtering of the measured temperature is an intrinsic property of the IPOM-based algorithm. Note that increasing the sampling frequency of a data acquisition system (i.e. increasing p) often leads to an amplification of the noise (i.e. an increase in σ_ϑ). Together with the relations from

Table 1, this means that reducing σ_Q by adjusting p is a non-trivial task in practice.

7. Algorithm applications

7.1. Laser welding

Laser welding is a common technique for joining materials. If one of the materials is transparent to the laser wavelength, the laser beam can be directed perpendicular to the interface from the side of the transparent material. The energy of the laser pulse penetrates the transparent material with insignificant energy losses and is absorbed in the interfacial region, which leads to the heating of the materials and the formation of the welding joint (Cvecek et al. [43]). The quality of the welding joint strongly depends on the temperature regime.

Consider an inverse problem of contact heat conduction in laser welding of dissimilar glass pieces 1 and 2. The pieces have the following thermal properties: $K_1 = 0.9$ W/(m °C), $k_1 = 5 \bullet 10^{-7}$ m^2/s and $K_2 = 0.6$ W/(m °C), $k_2 = 3 \bullet 10^{-7}$ m^2/s. The initial temperature is $T_{i1} = T_{i2} = 20$ °C. The laser pulse is focussed through the transparent piece 2 onto the interface $x = 0$. The specific power q of the laser pulse changes in the time interval from zero to $t_s = 8$ s due to the function $q/q_{max} = 2^{8/5}(t/t_s)^{4/5}(1 - t/t_s)^{4/5}$ describing a single symmetrical pulse with the peak $q_{max} = 2 \bullet 10^6$ W/m^2. A thermocouple is installed in the piece 1 in such a way that the distance between its measuring junction and the interface is $h = 1$ mm. The thermal contact resistance between the measuring junction and piece 1 leads to a delay in the thermocouple response, which is characterised by the time constant $\tau = t_s/10 = 0.8$ s. The temperature measurement is conducted with a frequency of 50 Hz, implying $p = 400$ temperature samples, and a standard deviation of the noise of 5 °C. Reconstruct the specific power q and contact temperature $T_1 = T_2$ assuming that the thermal contact between the pieces is perfect, while all the energy of the laser pulse is absorbed at the interface.

Fig. 8 presents the IPOM solution obtained by Eqs.(24),(25) with the functions Ψ and Φ from Eq.(22) corresponding to the perfect thermal contact conditions. The minimum deviation σ^* is reached at $n^* = 8$, i.e. q is approximated by a polynomial of order 7. The IPOM and exact curves agree well for q and T_1, with the exception of the end interval, where a slight deviation occurs. With SFSM of Eq.(33), q can generally be reconstructed, albeit with the noticeable disturbances caused by the noise. Attempts to reconstruct q using Eq.(29) indicate that SICM is not suitable here due to a large rational time step Δ^*. Note that these results should be treated as estimate since several factors are not considered, including phase changes in the pieces and temperature effects on their properties.

7.2. Sliding friction

It is known that when bodies slide against each other, mechanical energy is dissipated in the form of heat at their interface. The associated temperature changes affect the properties of the bodies including their tribological performance (Kennedy [44]). Therefore, the temperature aspect is of paramount importance in the development and use of friction systems, such as brakes, clutches and bearings.

Consider an inverse problem of heat conduction in a brake pad 1 sliding against a disc 2 during a single braking interaction (Bryant and Day [45]). The pad 1 comprises a multi-ingredient material with $K_1 = 4$ W/(m °C) and $k_1 = 3 \bullet 10^{-6}$ m^2/s. Its initial temperature is $T_{i1} = 20$ °C. The steel disc 2 has sufficient heat capacity to neglect the temperature rise in it during the braking process, implying a constant temperature of $T_2 = 20$ °C. If the mechanical energy is completely converted into heat, the specific power q of heat generation is equal to the product of the friction coefficient, contact pressure and sliding speed. The function $q/q_{max} = 5^{5/3}/2^{8/3}(t/t_s)^{1/3}(1 - t/t_s)^{4/3}$ simulates a fast increase in q in the start interval due to the increasing contact pressure, where the peak $q_{max} = 7 \bullet 10^6$ W/m^2 is reached at $t = t_s/5$, and a subsequent decrease in q to zero due to the decreasing sliding speed. The braking duration is $t_s = 0.6$ s. The imperfect thermal contact between the pad 1 and disc 2 is characterised by the heat generation coefficient $\alpha = 0.09$ and contact heat transfer coefficient $\gamma = 800$ W/(m^2 °C). A thermocouple is installed in the pad 1 with a measuring junction at distance $h = 0.5$ mm from the friction surface. The time constant of the thermocouple is $\tau = t_s/3 = 0.2$ s. The frequency of the temperature measurement is 500 Hz, resulting in $p = 300$ temperature samples. The standard deviation of the noise is 0.7 °C. Reconstruct the specific power q and the contact temperature T_1 of the pad 1.

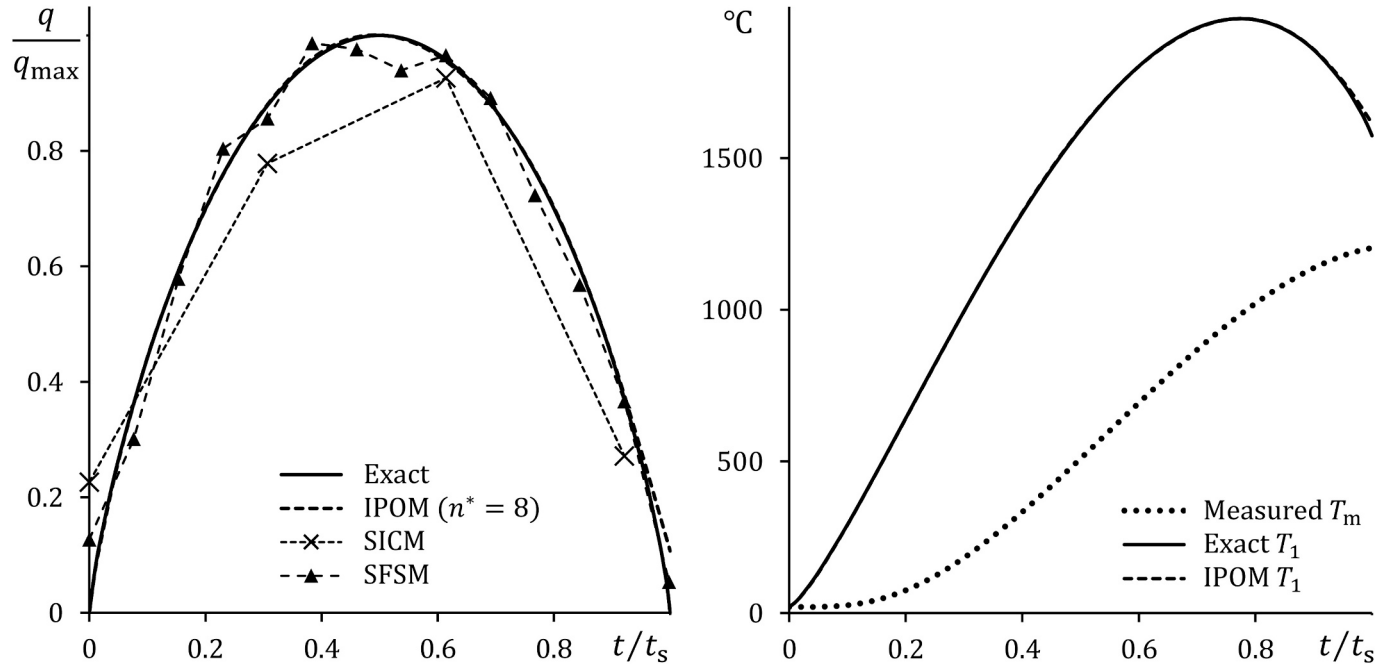

Fig. 8. Inverse problem of contact heat conduction in laser welding

Fig. 9 presents the IPOM solution according to Eqs.(24),(25) this time using the functions Ψ and Φ from Eq.(23) describing the imperfect thermal contact of a body with a constant-temperature counter-body. The IPOM solution corresponds to $n^* = 6$ and, accordingly, to a polynomial q of order 5. Despite the small deviations of the IPOM curve q from the exact curve, the overall character of q is not distorted, leading to an accurate reconstruction of T_1. It can also be seen that the SFSM solution by Eq.(33) is less accurate, while the SICM solution by Eq.(29) is not suitable at all.

7.3. Electric resistance welding

Electric resistance welding is a technique used to join materials by passing a controllable electric current through them. The passage of the current through the interface between the materials leads to thermoelectric processes associated with intensive heating and welding of the materials (Yang et al. [46]). As with laser welding, the temperature regime has a decisive influence on the quality of the welding joint.

Consider an inverse problem of contact heat conduction in electric resistance welding of similar pieces 1 and 2 made of an aluminium alloy. The thermal properties of the pieces are specified as $K_1 = K_2 = 200$ W/(m °C) and $k_1 = k_2 = 8 \bullet 10^{-5}$ m^2/s. The initial temperature of the piece 1 is $T_{i1} = 20$ °C, while the initial temperature $T_{i2} = 300$ °C of the piece 2 is higher due to the technological requirements. The specific power q of the heat generation changes due to a down-slope heat profile $q/q_{\max} = \sqrt{1 - t/t_s}$ with maximum $q_{\max} = 10^8$ W/m^2 at the initial time. The welding duration is short and equals $t_s = 0.1$ s. Since the pieces are made of the same material, the heat generation coefficient is reasonably assumed to be $\alpha = 1/2$. The surface roughness and oxide layers of the pieces imply imperfect thermal contact, which is characterised by the contact heat transfer coefficient $\gamma = 4000$ W/(m^2 °C). A thermocouple measures the temperature in the piece 1 at distance $h = 1$ mm from the interface. The time constant of the thermocouple is $\tau = 2t_s = 0.2$ s. Due to the short welding duration, a high sampling frequency of 5 kHz is set, providing $p = 500$ temperature samples, but with a stronger noise of standard deviation 2 °C. Reconstruct the specific power q and the contact temperatures T_1 and T_2 of the respective pieces 1 and 2.

Fig. 10 shows the specific power q and temperatures $T_{1,2}$ reconstructed by IPOM of Eqs.(24),(25) along with the functions Ψ and Φ in their general form of Eq.(19). It can be seen that a cubic approximation of q at $n^* = 4$ allows to accurately reconstruct $T_{1,2}$ for the noisy temperature measurement. The SFSM and SICM simulations by respective Eq.(33) and Eq.(29) are inadequate and cannot be shown due to a large rational time step Δ^*.

The obtained results suggest that the proposed IPOM-based algorithm allows to accurately reconstruct the heat fluxes and temperatures in two thermally coupled bodies from noisy measurements by a slow-response thermocouple, taking into account the interfacial heat source and initial temperature difference. The ratio τ/t_s is 1/10 for the laser welding problem (see Fig. 8) and 1/3 for the sliding friction problem (see Fig. 9) and is as large as 2 for the electric resistance welding problem (see Fig. 10). Further improvements of the algorithm may involve its combination with other advanced methods, such as those based on neural networks (Raudenský et al. [47]), genetic algorithms (Gosselin et al. [48]), fuzzy logic (Wang et al. [49]), particle swarm optimisation (Zálešák et al. [50]), etc.

8. Conclusions

An algorithm for solving the inverse problems of contact heat conduction has been developed based on the inverse parametric optimisation method. Using the Laplace integral transform, the impulse response function is derived for the direct problem of heat conduction in two bodies coupled with the imperfect thermal contact conditions, describing the interfacial heat source, heat partition and contact heat transfer. The thermocouple response is assumed to obey the first-order model with the time constant parameter. The specific power of the heat source is sought in the form of a polynomial providing the least-squares deviation of the simulated temperature from the temperature samples obtained by the thermocouple. The important particular cases of the imperfect thermal contact conditions, including the forced heat partition, perfect thermal contact and imperfect thermal contact of a body with a constant-temperature counter-body, are also treated. The accuracy of the algorithm and its noise robustness are analysed and compared to those for the classical methods of simple inverse convolution and sequential function specification.

The proposed algorithm proves to be accurate in a substantially larger variation region of the heating duration and time constant, covering also slow-response thermocouple measurements. This is attributed to the fact that the algorithm is free from the instability and

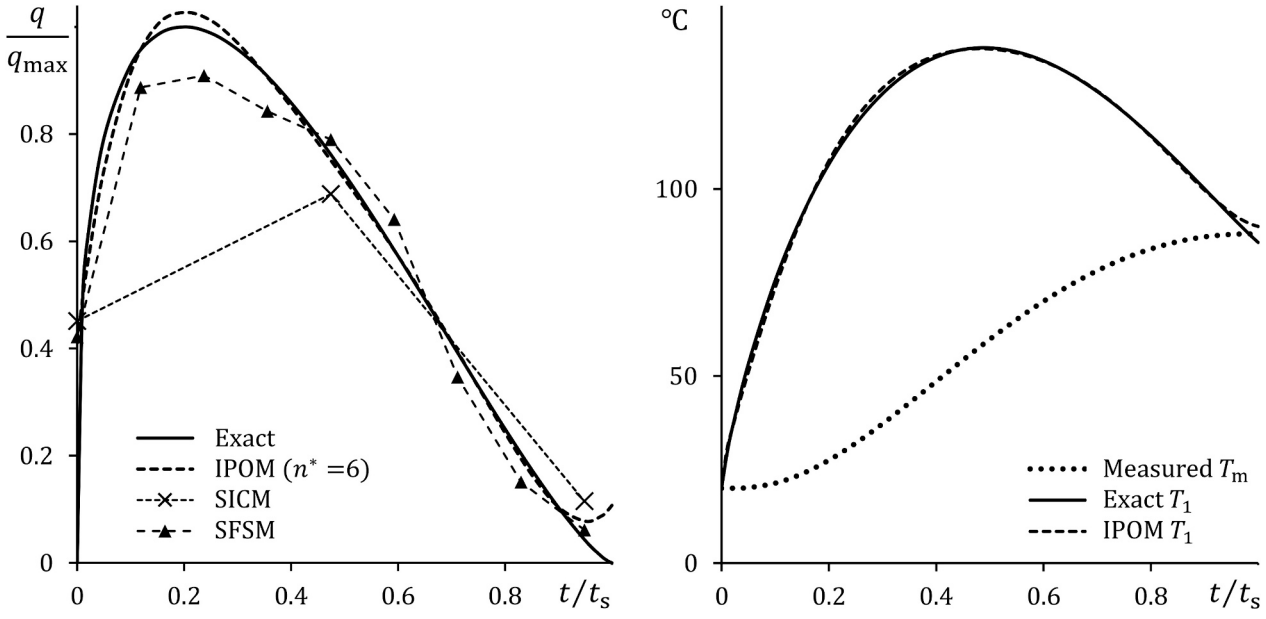

Fig. 9. Inverse problem of contact heat conduction in sliding friction

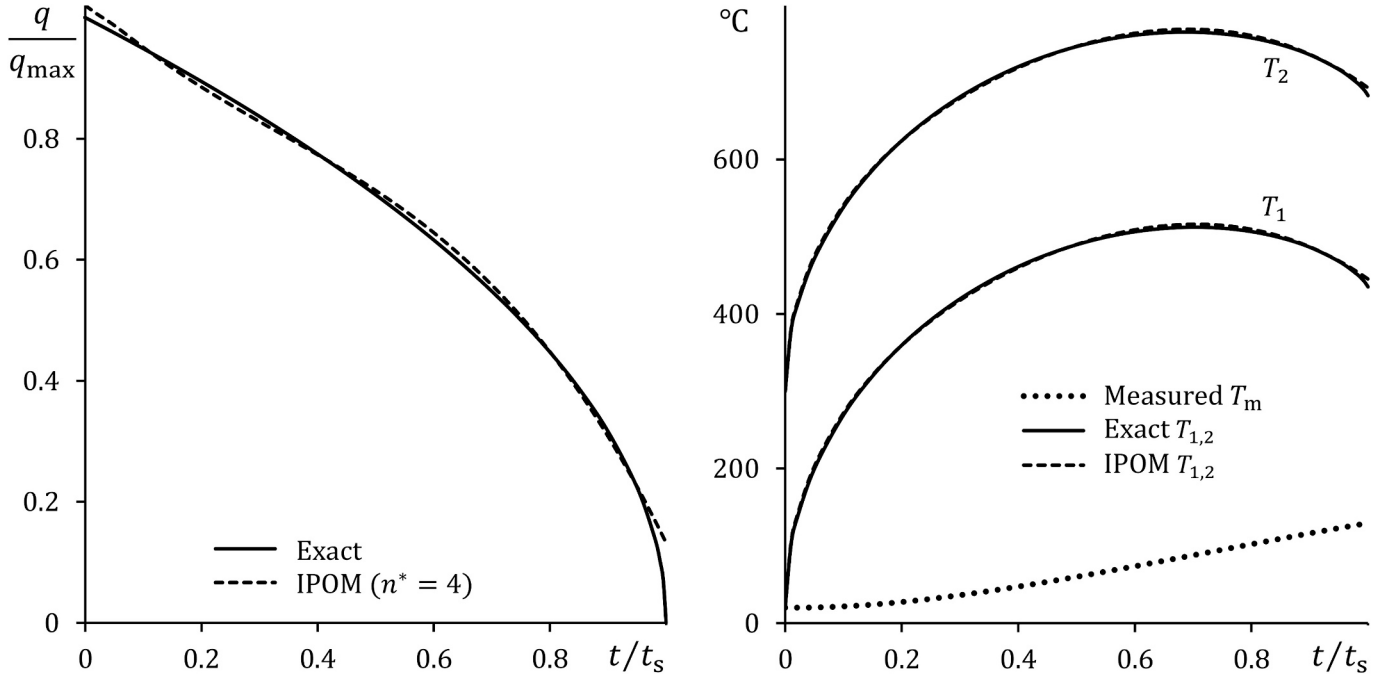

Fig. 10. Inverse problem of contact heat conduction in electric resistance welding

oversmoothing limitations inherent in the reference methods. Additionally, the algorithm is significantly more robust against noise with a sufficient number of temperature samples. The assumption of a polynomial specific power does not appear to be too restrictive in practice. Successful applications of the algorithm are demonstrated on the inverse contact heat conduction problems typical for sliding friction, laser and electric resistance welding. It becomes clear that the algorithm is able to accurately reconstruct the heat source specific power and contact temperatures from noisy temperature measurements for different ratios of the time constant to the heating duration.

CRediT authorship contribution statement

Oleksii Nosko: Conceptualization, Funding acquisition, Methodology, Investigation, Formal analysis, Validation, Writing – original draft, Writing – review & editing.

Declaration of competing interest

The author declares the following financial interests/personal relationships which may be considered as potential competing interests:

Oleksii Nosko reports financial support was provided by the National Science Centre, Poland.

Data availability

Data will be made available on request.

Acknowledgement

The present work was supported by the National Science Centre, Poland [grant number 2023/49/B/ST8/01979]. Computations were carried out at the Centre of Informatics Tricity Academic Supercomputer & Network (Poland). The author is grateful to an unknown Reviewer whose valuable comments helped to improve the manuscript.

Appendix A

Analytical expressions of the repeated integrals Ψ_j of the impulse response function for $j\in\{1,2,\ldots,10\}$ according to Eq.(20).

$$\Psi_j(\eta)=(j-1)!\left(\frac{\alpha\Lambda i+B\sqrt{\chi\Theta}}{2\left(B\Theta(\Lambda+\sqrt{\chi})i-\Lambda\sqrt{\Theta}\right)}\psi_j\left(\eta,-\frac{i}{\sqrt{\Theta}}\right)+\frac{\alpha\Lambda i-B\sqrt{\chi\Theta}}{2\left(B\Theta(\Lambda+\sqrt{\chi})i+\Lambda\sqrt{\Theta}\right)}\psi_j\left(\eta,\frac{i}{\sqrt{\Theta}}\right)+\frac{B\Lambda\left(\sqrt{\chi}-\alpha(\Lambda+\sqrt{\chi})\right)}{\Lambda^2+\Theta B^2(\Lambda+\sqrt{\chi})^2}\psi_j\left(\eta,\frac{B(\Lambda+\sqrt{\chi})}{\Lambda}\right)\right);$$

$$\psi_0(\eta,z)=exp\{z(1+z\eta)\}erfc\left\{\frac{1}{2\sqrt{\eta}}+z\sqrt{\eta}\right\};$$

$$\psi_1(\eta,z)=\frac{2\sqrt{\eta}exp\{-1/(4\eta)\}}{z\sqrt{\pi}}-(1+z)\frac{erfc\left\{1\Big/\left(2\sqrt{\eta}\right)\right\}}{z^2}+\frac{\psi_0(\eta,z)}{z^2};$$

$$\psi_2(\eta,z)=(3+z+4z\eta)\frac{\sqrt{\eta}exp\{-1/(4\eta)\}}{3z^2\sqrt{\pi}}-(3+z+6(1+z)\eta)\frac{erfc\left\{1\Big/\left(2\sqrt{\eta}\right)\right\}}{6z^2}+\frac{\psi_1(\eta,z)}{z^2};$$

$$\psi_3(\eta,z)=\left(5+z+2(25+9z)\eta+32z\eta^2\right)\frac{\sqrt{\eta}exp\{-1/(4\eta)\}}{60z^2\sqrt{\pi}}-\left(5+z+20(3+z)\eta+60(1+z)\eta^2\right)\frac{erfc\left\{1\Big/\left(2\sqrt{\eta}\right)\right\}}{120z^2}+\frac{\psi_2(\eta,z)}{z^2};$$

$$\psi_4(\eta,z)=\left(7+z+4(49+10z)\eta+12(77+29z)\eta^2+384z\eta^3\right)\frac{\sqrt{\eta}exp\{-1/(4\eta)\}}{2520z^2\sqrt{\pi}}-\left(7+z+42(5+z)\eta+420(3+z)\eta^2\right.$$
$$\left.+840(1+z)\eta^3\right)\frac{erfc\left\{1\Big/\left(2\sqrt{\eta}\right)\right\}}{5040z^2}+\frac{\psi_3(\eta,z)}{z^2};$$

$$\psi_5(\eta,z)=\left(9+z+2(243+35z)\eta+60(111+23z)\eta^2+24(837+325z)\eta^3+6144z\eta^4\right)\frac{\sqrt{\eta}exp\{-1/(4\eta)\}}{181440z^2\sqrt{\pi}}-\left(9+z+72(7+z)\eta+1512(5+z)\eta^2\right.$$
$$\left.+10080(3+z)\eta^3+15120(1+z)\eta^4\right)\frac{erfc\left\{1\Big/\left(2\sqrt{\eta}\right)\right\}}{362880z^2}+\frac{\psi_4(\eta,z)}{z^2};$$

$$\psi_6(\eta,z)=\left(11+z+4(242+27z)\eta+56(462+67z)\eta^2+240(968+203z)\eta^3+240(2123+843z)\eta^4+122880z\eta^5\right)\frac{\sqrt{\eta}exp\{-1/(4\eta)\}}{19958400z^2\sqrt{\pi}}-\left(11+z+110(9\right.$$
$$\left.+z)\eta+3960(7+z)\eta^2+55440(5+z)\eta^3+277200(3+z)\eta^4+332640(1+z)\eta^5\right)\frac{erfc\left\{1\Big/\left(2\sqrt{\eta}\right)\right\}}{39916800z^2}+\frac{\psi_5(\eta,z)}{z^2};$$

$$\psi_7(\eta,z)=\left(13+z+2(845+77z)\eta+72(1027+115z)\eta^2+336(3887+567z)\eta^3+1680(5161+1093z)\eta^4+1440(10309+4165z)\eta^5\right.$$
$$\left.+2949120z\eta^6\right)\frac{\sqrt{\eta}exp\{-1/(4\eta)\}}{3113510400z^2\sqrt{\pi}}-\left(13+z+156(11+z)\eta+8580(9+z)\eta^2+205920(7+z)\eta^3+2162160(5+z)\eta^4\right.$$
$$\left.+8648640(3+z)\eta^5+8648640(1+z)\eta^6\right)\frac{erfc\left\{1\Big/\left(2\sqrt{\eta}\right)\right\}}{6227020800z^2}+\frac{\psi_6(\eta,z)}{z^2};$$

$$\psi_8(\eta,z)=\left(15+z+4(675+52z)\eta+132(1325+121z)\eta^2+4320(1175+132z)\eta^3+15120(4413+647z)\eta^4+20160(17365+3708z)\eta^5\right.$$
$$\left.+20160(24285+9949z)\eta^6+82575360z\eta^7\right)\frac{\sqrt{\eta}exp\{-1/(4\eta)\}}{653837184000z^2\sqrt{\pi}}-\left(15+z+210(13+z)\eta+16380(11+z)\eta^2+600600(9+z)\eta^3\right.$$
$$\left.+10810800(7+z)\eta^4+90810720(5+z)\eta^5+302702400(3+z)\eta^6+259459200(1+z)\eta^7\right)\frac{erfc\left\{1\Big/\left(2\sqrt{\eta}\right)\right\}}{1307674368000z^2}+\frac{\psi_7(\eta,z)}{z^2};$$

$$\psi_9(\eta,z)=\left(17+z+2(2023+135z)\eta+52(6987+539z)\eta^2+264(59245+5421z)\eta^3+23760(14263+1607z)\eta^4+30240(117045+17237z)\eta^5\right.$$
$$\left.+60480(253181+54445z)\eta^6+40320(447661+185517z)\eta^7+2642411520z\eta^8\right)\frac{\sqrt{\eta}exp\{-1/(4\eta)\}}{177843714048000z^2\sqrt{\pi}}-\left(17+z+272(15+z)\eta\right.$$
$$\left.+28560(13+z)\eta^2+1485120(11+z)\eta^3+40840800(9+z)\eta^4+588107520(7+z)\eta^5+4116752640(5+z)\eta^6+11762150400(3+z)\eta^7\right.$$
$$\left.+8821612800(1+z)\eta^8\right)\frac{erfc\left\{1\Big/\left(2\sqrt{\eta}\right)\right\}}{355687428096000z^2}+\frac{\psi_8(\eta,z)}{z^2};$$

$$\psi_{10}(\eta,z)=\left(19+z+4(1444+85z)\eta+120(5719+382z)\eta^2+4368(9386+725z)\eta^3+13728(96140+8813z)\eta^4+95040(239704+27079z)\eta^5\right.$$
$$\left.+1330560(148105+21898z)\eta^6+1209600(598538+129503z)\eta^7+725760(1014239+424415z)\eta^8\right.$$
$$\left.+95126814720z\eta^9\right)\frac{\sqrt{\eta}exp\{-1/(4\eta)\}}{608225502044160002^2\sqrt{\pi}}-\left(19+z+342(17+z)\eta+46512(15+z)\eta^2+3255840(13+z)\eta^3\right.$$
$$\left.+126977760(11+z)\eta^4+2793510720(9+z)\eta^5+33522128640(7+z)\eta^6+201132771840(5+z)\eta^7+502831929600(3+z)\eta^8\right.$$
$$\left.+335221286400(1+z)\eta^9\right)\frac{erfc\left\{1\Big/\left(2\sqrt{\eta}\right)\right\}}{121645100408832000z^2}+\frac{\psi_9(\eta,z)}{z^2}$$

References

[1] J.V. Beck, B. Blackwell, C.R. St, Clair, Inverse Heat Conduction: Ill-Posed Problems, Wiley-Interscience, New York, 1985.

[2] K.A. Woodbury, H. Najafi, F. de Monte, J.V. Beck, Inverse heat conduction problems: An overview, in: K.A. Woodbury, H. Najafi, F. de Monte, J.V. Beck (Eds.), Inverse Heat Conduction: Ill-Posed Problems, John Wiley & Sons, Inc, 2023, pp. 1–23, https://doi.org/10.1002/9781119840220.ch1.

[3] M. Zálešák, L. Klimeš, P. Charvát, M. Cabalka, J. Kůdela, T. Mauder, Solution approaches to inverse heat transfer problems with and without phase changes: a state-of-the-art review, Energy 278 B (2023) 127974, https://doi.org/10.1016/j.energy.2023.127974.

[4] W.L. Chen, Y.C. Yang, S.S. Chu, Estimation of heat generation at the interface of cylindrical bars during friction process, Appl. Therm. Eng. 29 (2009) 351–357, https://doi.org/10.1016/j.applthermaleng.2008.03.001.

[5] S.K. Wang, H.L. Lee, Y.C. Yang, Inverse problem of estimating time-dependent heat generation in a frictional heated strip and foundation, Int. Commun. Heat Mass Transf. 36 (2009) 925–930, https://doi.org/10.1016/j.icheatmasstransfer.2009.07.001.

[6] W.L. Chen, Y.C. Yang, Inverse prediction of frictional heat flux and temperature in sliding contact with a protective strip by iterative regularization method, Appl. Math. Model. 35 (2011) 2874–2886, https://doi.org/10.1016/j.apm.2010.11.068.

[7] J.G. Bauzin, N. Keruzore, N. Laraqi, A. Gapin, J.F. Diebold, Identification of the heat flux generated by friction in an aircraft braking system, Int. J. Therm. Sci. 130 (2018) 449–456, https://doi.org/10.1016/j.ijthermalsci.2018.05.008.

[8] J.G. Bauzin, M.N. Nguyen, N. Laraqi, M.B. Cherikh, Thermal characterization of frictional interfaces using experiments and inverse heat conduction methods, Int. J. Therm. Sci. 137 (2019) 431–437, https://doi.org/10.1016/j.ijthermalsci.2018.12.004.

[9] M.B. Cherikh, J.G. Bauzin, N. Laraqi, Experimental estimation of transient evolution of three thermal parameters characterizing a dry friction interface, Int. J. Heat Mass Transf. 169 (2021) 120986, https://doi.org/10.1016/j.ijheatmasstransfer.2021.120986.

[10] M. Gostimirovic, M. Sekulic, M. Trifunovic, M. Madic, D. Rodic, Stability analysis of the inverse heat transfer problem in the optimization of the machining process, Appl. Therm. Eng. 195 (2021) 117174, https://doi.org/10.1016/j.applthermaleng.2021.117174.
[11] K.A. Woodbury, Effect of thermocouple sensor dynamics on surface heat flux predictions obtained via inverse heat transfer analysis, Int. J. Heat Mass Transf. 33 (12) (1990) 2641–2649, https://doi.org/10.1016/0017-9310(90)90200-E.
[12] S. Augustin, T. Fröhlich, C. Ament, T. Güther, K. Irrgang, L. Lippmann, Dynamic properties of contact thermometers for high temperatures, Measurement 51 (2014) 387–392, https://doi.org/10.1016/j.measurement.2013.11.021.
[13] J.I. Frankel, H. Chen, Analytical developments and experimental validation of a thermocouple model through an experimentally acquired impulse response function, Int. J. Heat Mass Transf. 141 (2019) 1301–1314, https://doi.org/10.1016/j.ijheatmasstransfer.2019.05.098.
[14] O. Nosko, Y. Tsybrii, Inverse determination of sliding surface temperature based on measurements by thermocouples with account of their thermal inertia, Tribol. Int. 164 (2021) 107200, https://doi.org/10.1016/j.triboint.2021.107200.
[15] A.V.S. Oliveira, A. Avrit, M. Gradeck, Thermocouple response time estimation and temperature signal correction for an accurate heat flux calculation in inverse heat conduction problems, Int. J. Heat Mass Transf. 185 (2022) 122398, https://doi.org/10.1016/j.ijheatmasstransfer.2021.122398.
[16] C.F. Gomez, R. Nieuwenhuizen, C.W.M. van der Geld, H.G.M. Kuerten, M. Bsibsi, B. P.M. van Esch, Inaccuracies in the inverse heat conduction problem solution and their effect on the estimation of heat fluxes during quenching, Int. J. Heat Mass Transf. 194 (2022) 122953, https://doi.org/10.1016/j.ijheatmasstransfer.2022.122953.
[17] A.Y.C. Nee, A.O. Tay, On the measurement of surface grinding temperature, Int. J. Machine Tool Design Res. 21 (1981) 279–291, https://doi.org/10.1016/0020-7357(81)90025-1.
[18] A. Lefebvre, F. Lanzetta, P. Lipinski, A.A. Torrance, Measurement of grinding temperatures using a foil/workpiece thermocouple, Int. J. Mach. Tools Manuf. 58 (2012) 1–10, https://doi.org/10.1016/j.ijmachtools.2012.02.006.
[19] P.A. Santoni, T. Marcelli, E. Leoni, Measurement of fluctuating temperatures in a continuous flame spreading across a fuel bed using a double thermocouple probe, Combust. Flame 131 (1–2) (2002) 47–58, https://doi.org/10.1016/S0010-2180(02)00391-7.
[20] Q. Huang, L. Yue, X. Li, P. Wang, A correlation to calculate time constant of thermocouples, Appl. Therm. Eng. 246 (2024) 122920, https://doi.org/10.1016/j.applthermaleng.2024.122920.
[21] M. Jaremkiewicz, D. Taler, T. Sobota, Measuring transient temperature of the medium in power engineering machines and installations, Appl. Therm. Eng. 29 (2009) 3374–3379, https://doi.org/10.1016/j.applthermaleng.2009.05.013.
[22] Y. Zhang, X. Li, C. Li, W. Wu, J. Wang, Development of exposed rapid thermocouple for internal fluid temperature testing under pressure, Appl. Therm. Eng. 216 (2022) 119130, https://doi.org/10.1016/j.applthermaleng.2022.119130.
[23] A. Terzis, J. von Wolfersdorf, B. Weigand, P. Ott, Thermocouple thermal inertia effects on impingement heat transfer experiments using the transient liquid crystal technique, Meas. Sci. Technol. 23 (2012) 115303, https://doi.org/10.1088/0957-0233/23/11/115303.
[24] J.I. Sylvia, S. Clement Ravi Chandar, K. Velusamy, A novel method for in-situ estimation of time constant for core temperature monitoring thermocouples of operating reactors, Nucl. Eng. Des. 275 (2014) 154–162, https://doi.org/10.1016/j.nucengdes.2014.04.007.
[25] S. Sridhar, A.K. Saha, K. Vinolia, A. Babu, K.V. Sureshkumar, Performance of core thermocouples of FBTR – a technique for predicting accurate temperature for known transients in the presence of measurement delays, Nucl. Eng. Des. 340 (2018) 260–274, https://doi.org/10.1016/j.nucengdes.2018.07.002.
[26] M. Tagawa, Y. Ohta, Two-thermocouple probe for fluctuating temperature measurement in combustion – rational estimation of mean and fluctuating time constants, Combust. Flame 109 (1997) 549–560, https://doi.org/10.1016/S0010-2180(97)00044-8.
[27] D. Taler, T. Sobota, M. Jaremkiewicz, J. Taler, Influence of the thermometer inertia on the quality of temperature control in a hot liquid tank heated with electric energy, Energies 13 (2020) 4039, https://doi.org/10.3390/en13154039.
[28] G. Doetsch, Introduction to the Theory and Application of the Laplace Transformation, Springer, Berlin, 1974, https://doi.org/10.1007/978-3-642-65690-3.
[29] S.A. Schaaf, On the superposition of a heat source and contact resistance, Q. Appl. Math. 5 (1) (1947) 107–111.
[30] W.A. Mersman, Heat conduction in an infinite composite solid with an interface resistance, Trans. Am. Math. Soc. 53 (1) (1943) 14–24, https://doi.org/10.2307/1990129.
[31] H.S. Carslaw, J.C. Jaeger, Conduction of Heat in Solids, 2nd ed., Oxford University Press, London, 1959, p. 496.
[32] A.A. Yevtushenko, M. Kuciej, One-dimensional thermal problem of friction during braking: the history of development and actual state, Int. J. Heat Mass Transf. 55 (15–16) (2012) 4148–4153, https://doi.org/10.1016/j.ijheatmasstransfer.2012.03.056.
[33] O. Nosko, Thermal boundary conditions to simulate friction layers and coatings at sliding contacts, Int. J. Heat Mass Transf. 127 A (2018) 1128–1137, https://doi.org/10.1016/j.ijheatmasstransfer.2018.06.027.
[34] J.V. Beck, Calculation of surface heat flux from an internal temperature history. ASME Paper 62-HT-46, 1962.
[35] I. Frank, An application of least squares method to the solution of the inverse problem of heat conduction, J. Heat Transf. 85 (4) (1963) 378–379, https://doi.org/10.1115/1.3686128.
[36] O.R. Burggraf, An exact solution of the inverse problem in heat conduction theory and applications, J. Heat Transf. 86 (3) (1964) 373–380, https://doi.org/10.1115/1.3688700.
[37] K.A. Woodbury, J.V. Beck, Estimation metrics and optimal regularization in a Tikhonov digital filter for the inverse heat conduction problem, Int. J. Heat Mass Transf. 62 (2013) 31–39, https://doi.org/10.1016/j.ijheatmasstransfer.2013.02.052.
[38] G. Stolz, Numerical solutions to an inverse problem of heat conduction for simple shapes, J. Heat Transf. 82 (1) (1960) 20–25, https://doi.org/10.1115/1.3679871.
[39] J.V. Beck, Thermocouple temperature disturbances in low conductivity materials, J. Heat Transf. 84 (2) (1962) 124–131, https://doi.org/10.1115/1.3684310.
[40] O.M. Alifanov, Inverse heat transfer problems, Springer, Berlin, 1994, pp. 103–117, https://doi.org/10.1007/978-3-642-76436-3.
[41] J.V. Beck, Surface heat flux determination using an integral method, Nucl. Eng. Des. 7 (2) (1968) 170–178, https://doi.org/10.1016/0029-5493(68)90058-7.
[42] J.V. Beck, Nonlinear estimation applied to the nonlinear inverse heat conduction problem, Int. J. Heat Mass Transf. 13 (1970) 703–716.
[43] K. Cvecek, S. Dehmel, I. Miyamoto, M. Schmidt, A review on glass welding by ultra-short laser pulses, Int. J. Extreme Manufact. 1 (2019) 042001, https://doi.org/10.1088/2631-7990/ab55f6.
[44] F.E. Kennedy, Thermal and thermomechanical effects in dry sliding, Wear 100 (1984) 453–476, https://doi.org/10.1016/0043-1648(84)90026-7.
[45] D. Bryant, A. Day, Chapter 8 — Thermal effects in friction brakes, in: D. Bryant, A. Day (Eds.), Braking of Road Vehicles, 2nd ed, Butterworth-Heinemann, 2022, pp. 277–323, https://doi.org/10.1016/B978-0-12-822005-4.00003-2.
[46] Y. Yang, Z. Luo, Y. Zhang, J. Su, Dissimilar welding of aluminium to steel: a review, J. Manuf. Process. 110 (2024) 376–397, https://doi.org/10.1016/j.jmapro.2023.12.060.
[47] M. Raudenský, J. Horský, J. Krejsa, Usage of neural network for coupled parameter and function specification inverse heat conduction problem, Int. Commun. Heat Mass Transf. 22 (5) (1995) 661–670, https://doi.org/10.1016/0735-1933(95)00052-Z.
[48] L. Gosselin, M. Tye-Gingras, F. Mathieu-Potvin, Review of utilization of genetic algorithms in heat transfer problems, Int. J. Heat Mass Transf. 52 (9–10) (2009) 2169–2188, https://doi.org/10.1016/j.ijheatmasstransfer.2008.11.015.
[49] G. Wang, L. Zhu, H. Chen, A decentralized fuzzy inference method for solving the two-dimensional steady inverse heat conduction problem of estimating boundary condition, Int. J. Heat Mass Transf. 54 (13–14) (2011) 2782–2788, https://doi.org/10.1016/j.ijheatmasstransfer.2011.01.032.
[50] M. Zálešák, P. Charvát, L. Klimeš, Identification of the effective heat capacity–temperature relationship and the phase change hysteresis in PCMs by means of an inverse heat transfer problem solved with metaheuristic methods, Appl. Therm. Eng. 197 (2021) 117392, https://doi.org/10.1016/j.applthermaleng.2021.117392.